ELSEVIER

Journal of Nuclear Materials 244 (1997) 75–84

journal of nuclear materials

Finite volume method for fission gas release modeling

L.C. Bernard *, E. Bonnaud

Framatome, 10 Rue Juliette Récamier, 69456 Lyon cedex 06, France

Received 21 February 1996; accepted 5 November 1996

Abstract

A finite volume method is presented to analyze the fission gas release from UO_2 fuel during Light Water Reactor normal or off-normal operations, the latter being limited to Class-II type incidents. The model assumes gas diffusion inside a spherical grain under time-varying conditions. It also uses a time-varying imperfect sink condition at the grain boundary due to the accumulation of gas by irradiation-induced re-solution. The onset of gas release occurs due to the saturation of the gas amount in the grain boundaries. The problem is efficiently solved by a fast numerical technique which uses finite volumes, well-suited for application in fuel rod analyses computer codes.

1. Introduction

The release of stable fission gases from UO_2 fuel is important in predicting fuel rod performance during Light Water Reactor (LWR) operation. Gas release increases the fuel rod internal pressure and temperature by degrading the pellet-cladding gap conductance. Both effects must be minimized for safe fuel rod performance.

Fission gas release is a complex phenomenon, involving many mechanisms (see for instance Ref. [1]). It can be divided into an athermal regime and a thermally-activated regime. Athermal release is the result of gas atom motion by recoil and knock-out which escape through the free surfaces of the fuel. Its amplitude remains low except at high burnups in the rim region. This type of release will not be dealt with in this paper.

Thermal release is observed above a temperature 'incubation' threshold that decreases with burnup [2]. This threshold can be identified by the presence of inter-granular gas, most often observed as lenticular bubbles, whose radius is a fraction of one micron. Gas atoms diffuse from the center of UO_2 grains towards grain boundaries with a velocity that increases with temperature. Initially, these atoms accumulate at the grain boundaries and there is no release. When the number of gas atoms per unit area, N, reaches a saturation value, N_S, there is the onset of the gas release.

The presence of inter-granular gas introduces another phenomenon. Fission spikes bring back into solution a fraction of inter-granular atoms. This induces a 're-solution' flux which counter-acts in part the flux diffusion. Re-solution is also acting inside the grains where atoms cluster into fine bubbles made of a few atoms and whose radius is $\sim 10^{-9}$ m. These bubbles are brought back into solution, recombination and re-solution balancing out.

Since the pioneering work of Booth [3] and Speight [4], there is a well-established mathematical framework to solve the above-mentioned diffusion problem. Booth derived analytical expressions for constant irradiation conditions in two cases relevant to LWR operations: (i) the constant gas production case relevant to steady-state operation, and (ii) the zero gas production case which is more relevant to transient operation (load-follow and incidents) when the power level is high enough for the gas production to be neglected with respect to diffusion release. This study was limited to a perfect sink boundary condition where there is a release as soon as gas atoms reach the grain boundary, or expressed mathematically, the concentration at the grain boundary is zero. Speight improved this Booth model by introducing re-solution. Then, there is an imperfect sink condition where the concentration at the

* Corresponding author. Tel.: +33-4 72 74 72 94; fax: +33-4 72 74 88 33.

PII S0022-3115(96)00720-9

grain boundary remains finite. A closed form analytical solution of the model is given by Turnbull [5].

Later works [6–18] treat the general problem of time-varying conditions. There is no closed form analytical solution to this problem and the problem is solved either with a numerical approach or a semi-analytical approach. Both approaches have their merits and drawbacks. In principle, with a numerical approach, one can obtain the required accuracy by increasing the number of meshes and/or time-steps, at the expense of computer time. The other approach is computer-time efficient but may not be accurate enough for all situations.

Here, we present a new method which combines the advantages of both approaches. It is numerical but fast enough to compete with semi-analytical methods. It is based on the finite-volume method for space discretization.

To be more specific, Section 2 describes the physical model. It is important to know the order of magnitude of the physical quantities in order to look for the numerical algorithm that is best suited to the physical problem. Although we want an algorithm that is accurate for a wide range of conditions, we restrict ourselves to all situations encountered in LWR normal operations and off-normal operations that are limited to Class-II incidents. Section 3 presents the numerical technique. Several algorithms have been tried for space and time discretization. An optimal choice was found. The results are presented in Section 4. The method is initially tested with three constant condition cases which have analytical solutions. These cases provided a means of evaluating the power of the method. The results of numerical cases with time-varying conditions are then presented. The results are discussed in Section 5, together with other numerical schemes. A conclusion is presented in Section 6.

2. The model

2.1. Introduction

The model is based on previous closely related models considered by several previous investigators [4–6,12–17]. Gas release is calculated by modeling one UO_2 grain. The grain shape is idealized by a spherical shape. Gas release is a two-step diffusion process from the interior of the grain to the grain boundary. In the first step, gas atoms accumulate at the grain boundary without release. In the second step, gas release is activated when the gas density at the boundary is bigger than at saturation density. The problem is then to solve a diffusion equation inside the grain with a time-varying condition at the grain boundary.

This Section is devoted to formulate the ensuing mathematical problem. First, the expressions and/or orders of magnitude of key physical parameters are given, namely, the grain size, the diffusion coefficient of Xenon inside UO_2, and the saturation density. It is important to know the range of these parameters to find an efficient algorithm for solving the mathematical problem.

2.2. Grain size

Observations indicate that grain growth occurs at elevated temperatures in agreement with grain growth models [19]. However, we have chosen to model the grain size as constant. This approach was taken with for simplification and because grain growth induces opposite effects. On one hand, grain growth tends to lower diffusion and hence gas release. To rigorously treat the problem, one must tackle the more difficult task of solving the diffusion equation with a moving boundary [20]. On the other hand, grain growth causes a sweeping of the gas accumulated on the grain boundaries which enhances the gas release. Computations though have shown [21] that gas release is higher with constant grain size and no gas sweeping than when both effects of grain growth and gas sweeping are taken into account.

2.3. Diffusion coefficient

We follow the formalism of Turnbull et al. [22,23]. In this formalism, the diffusion coefficient, D, is the sum of three components D_1, D_2, and D_3. The D_1 term represents the intrinsic diffusion in the absence of irradiation. The D_2 and D_3 terms represent the thermal and athermal contributions induced by irradiation, respectively. A correction due to the irradiation-induced re-solution of intragranular bubbles is, according to Ref. [4]:

$$D = \frac{D_{1+2+3}}{1 + g/b'}, \tag{1}$$

where

$$D_{1+2+3} = D_1 + D_2 + D_3 \tag{2}$$

and g and b' are the probabilities of trapping atoms within intra-granular bubbles and of re-solution of these atoms by fission spikes. The random-walk formula [1] gives

$$g = D_{1+2+3}/L^2, \tag{3}$$

where L is the mean free-path between two bubbles. Eqs. (1) and (3) yield

$$D = \frac{1}{1/(D_{1+2+3}) + 1/(L^2 b')}. \tag{4}$$

The preceding expression indicates that D attains a saturation value of L^2b' at high temperatures. The expressions for the diffusion coefficient terms are

$$D_1 = D_{01}\exp\left(\frac{-T_{01}}{T_K}\right), \tag{5}$$

$$D_2 = D_{02}\exp\left(\frac{-T_{02}}{T_K}\right)\sqrt{\frac{P'}{20}}, \tag{6}$$

$$D_3 = D_{03}\frac{P'}{20}, \tag{7}$$

where T_K is the local temperature (K) and P' is the linear heat generation rate (LHGR) expressed in kW/m units. The following values [22–24] were chosen where D is expressed in m^2/s units: $D_{01} = 3.9\times10^{-6}$ m^2/s, $T_{01} = 45275$ K, $D_{02} = 1.77\times10^{-15}$ m^2/s, $T_{02} = 13800$ K, $D_{03} = 4\times10^{-21}$ m^2/s, $L^2b' = 10^{-15}$ m^2/s.

2.4. The incubation threshold

The incubation threshold is obtained from theoretical and experimental considerations. The theoretical background follows [12]. Fission spikes bring back into solution part of the gas contained within inter-granular bubbles. The corresponding re-solution flux is

$$J_{rs} = (bN)/2, \tag{8}$$

where b is the probability of re-solution of the inter-granular atoms, N is the density per unit area at the grain boundaries. An expression for the mean concentration at the grain boundaries, c_δ, is obtained by assuming that the re-solution flux is close to the diffusion flux. From Fick's law, the diffusion flux $D\nabla c \sim (Dc_\delta)/\delta$ where c_δ is the width of the re-solution layer at the grain boundaries. Hence

$$c_\delta = (bN\delta)/(2D). \tag{9}$$

Moreover, following Ref. [4], the flux out of the grain is of the form

$$J = J_0(1 - c_\delta/(\beta t)), \tag{10}$$

where β is the creation rate and J_0 is the flux in the absence of re-solution. This flux, J_0, for a spherical grain of radius a is

$$J_0 = \frac{1}{4\pi a^2}\frac{d}{dt}\left[\frac{4}{3}\pi a^3\beta t F_0\right], \tag{11}$$

where F_0 is the gas release fraction in the absence of re-solution. The Booth diffusion model [3] gives an approximate solution for low releases:

$$F_0 \sim \frac{4}{\sqrt{\pi}}\frac{\sqrt{Dt}}{a}. \tag{12}$$

Finally, the evolution of the surface density at the grain boundaries is obtained from the following equation:

$$\frac{d}{dt}N = 4\beta\frac{\sqrt{Dt}}{\sqrt{\pi}}\left(1 - \frac{Nb\delta}{2D\beta t}\right). \tag{13}$$

The incubation time, t_i, is given by the solution of the previous equation for $t_i = t(N_S)$ where N_S is the threshold value of the surface density. When D is constant with time, two asymptotic solutions of this equation at low and high temperatures are obtained:

$$T_{low}: t_i \sim (bN_S\delta)/(2D\beta),$$

$$T_{high}: t_i \sim \left(\frac{9}{8\pi}\right)^{1/3}\left(\frac{N_S}{\beta}\right)^{2/3}\frac{1}{D^{1/3}}. \tag{14}$$

The expression of the incubation burnup $B_i \sim \beta t_i/(6.9\times10^{21})$ can be deduced from Eqs. (1)–(7) of the diffusion coefficient. At low temperatures

$$B_i \sim \frac{bN_S\delta}{2(D_2 + D_3)}, \tag{15}$$

and at high temperatures

$$B_i \sim \left(\frac{9}{8\pi}\right)^{1/3}(N_S)^{2/3}\beta^{1/3}\left(\frac{1}{D_1} + L^2b'\right)^{1/3}. \tag{16}$$

Two important remarks enable one to combine these two asymptotic expressions in one single expression. On the one hand,

$$T_{02} \sim T_{01}/3. \tag{17}$$

On the other hand, there are great uncertainties for the values of the parameters b, δ and N_S and, a fortiori, on the combination of these parameters. We therefore seek a solution for the incubation threshold of the form

$$B_i = \frac{B_1}{\exp(-T_B/T_K) + B_2(T_K - B_3)} + B_{MIN}, \tag{18}$$

where T_K = local temperature (K), $T_B = T_{02} = 13800$ K. The parameters B_1, B_2, B_3, and B_{MIN} are the adjustable parameters of the model, in agreement with experimental fission gas release results. The initial values of these parameters were taken from the usual values found in literature. The following set of parameters proved to be a reasonable experimental fit: $B_1 = 1$ MWd/tM, $B_2 = 3.3\times$

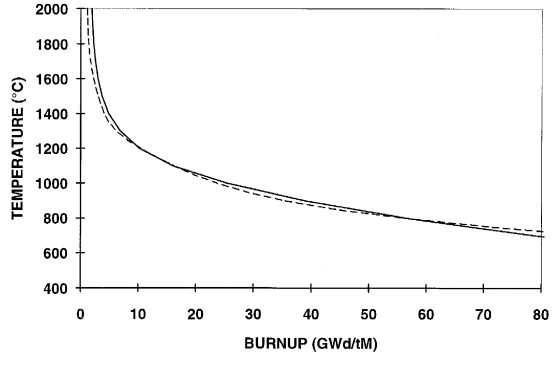

Fig. 1. Incubation threshold. The solid line is given by Eq. (18). The dashed line is given by Eq. (13).

10^{-8} K^{-1}, $B_3 = 603$ K, $B_{MIN} = 1500$ MWd/tM, $T_B = 13800$ K. Fig. 1 shows the evolution of the thermal threshold, as given by Eq. (18).

The order of magnitude of N_S can be estimated [13] by supposing that inter-granular atoms cluster into lenticular bubbles. The parameters of the bubble shape are, the radius R_B, the volume V_B, and the dihedral angle 2θ. Ideal gas law links the bubble pressure, P, and the number of atoms, n, in a bubble:

$$PV_B = nkT. \tag{19}$$

The following relations hold:

$$n_B n = N_S, \tag{20}$$

$$n_B = F_B/\pi R_B^2 \sin^2\theta, \tag{21}$$

$$P = P_{EXT} + 2\gamma/R_B, \tag{22}$$

$$V_B = (4\pi/3) R_B^3 f(\theta), \tag{23}$$

$$f(\theta) = 1 - \tfrac{3}{2}\cos\theta + \tfrac{1}{2}\cos^3\theta, \tag{24}$$

where n_B is the number of bubbles per m^2, F_B is the fractional coverage of bubbles (i.e., the ratio of the area occupied by bubbles to the grain area), and P is the sum of the surface tension and of the other contributions (hydrostatic, mechanical stresses). These expressions allow one to deduce the following equality for N_S:

$$N_S = \left[4f(\theta)/3kT\sin^2\theta)\right](P_{EXT} + 2\gamma/R_B) R_B F_B. \tag{25}$$

Not all quantities in Eq. (25) are well known. Most analyses assume $\gamma = 1$ J m^{-2}, $R_B = 0.5$ μ, $F_B = 0.25$, $\theta = 50°$ and then $f(\theta)/\sin^2\theta = 0.288$. The pressure is the least-well known term. Between the two limiting cases $P_{EXT} = 0$ (then, $P = 4$ MPa) and $P_{EXT} \sim 120$ MPa (UO_2 fracture threshold [25]): N_S varies from 10^{19} m^{-2} (similar to the value given by a mono-atomic layer) to 3×10^{20} m^{-2}. From Ref. [26], P is close (~ 90 MPa) to the upper limit, in agreement with the values of N_S reported in Ref. [27] (a few 10^{-20} m^{-2}). The dashed curve of Fig. 1 represents the solution of Eq. (13) for the expressions of the diffusion coefficient presented in Eqs. (1)–(7) and the following values of $N_S = 3 \times 10^{20} 1273/T_K$ m^{-2} and $b = 2 \times 10^{-6}$ s^{-1}. With this choice, both curves in Fig. 1 were found to match closely.

The gas equation of state differs slightly from the ideal gas law (Eq. (19)) for the preceding values of parameters. However, the order of magnitude of N_S is the same. For instance, one finds $N_S = 2 \times 10^{20}$ m^{-2} instead of 3×10^{20} m^{-2} by using a hard sphere equation of state [28].

2.5. The diffusion equation

Gas release follows the kinetics of diffusion from the interior of the grain towards the grain boundary. This mechanism is described with the classical model of an equivalent sphere of radius a.

The diffusion equation can be expressed as

$$\frac{\partial c}{\partial t} = \beta + \mathrm{div}(D\,\mathrm{grad}(c)), \tag{26}$$

where $c(r, t)$ is the local concentration (number of gas atoms per unit volume) and r is the space variable.

The boundary condition is given by Eq. (9).

3. The finite volume method

3.1. Introduction

The finite volume method consists in integrating the equation to be solved over control volumes and then discretizing the integral form. It has several attractive features. It ensures conservation of the integrated quantities, a fundamental property to respect in physics. It combines the simplicity of finite differences with the flexibility of finite elements.

Since the grain size is small, D can be assumed to be space-independent. Then, the diffusion equation (Eq. (26)) can be simplified with the following change of time variable

$$\tau = \int_0^t \frac{D}{a^2}\,\mathrm{d}t' \tag{27}$$

to read

$$\frac{\partial c}{\partial \tau} - \mathrm{div}[\mathrm{grad}(c)] = \beta'. \tag{28}$$

In Eq. (28), the creation rate is normalized from β to $\beta' = \beta a^2/D$ and r is normalized to $x = r/a$.

The integral form of Eq. (28) over a control-volume is

$$\frac{\partial}{\partial \tau}\int_{x'_i}^{x'_{i+1}} c x^2\,\mathrm{d}x - x'^2_{i+1}\left.\frac{\partial c}{\partial x}\right|_{x'_{i+1}} + x'^2_i\left.\frac{\partial c}{\partial x}\right|_{x'_i} = \int_{x'_i}^{x'_{i+1}} \beta' x^2\,\mathrm{d}x. \tag{29}$$

Control-volumes are iso-volumes. Denoting the boundaries (node points) of control-volume i by x'_i and x'_{i+1} and the number of control-volumes by N_x:

$$x'_{i+1} = \left(\frac{i}{N_x}\right)^{1/3}. \tag{30}$$

The mesh points, x_i, are located at a mid-distance between the node points:

$$x_i = 0.5(x'_i + x'_{i+1}). \tag{31}$$

3.2. Space discretization

3.2.1. Low-order scheme

This is the standard scheme. It consists of differencing the spatial-derivative term as follows:

$$\left.\frac{\partial c}{\partial x}\right|_{x'_i} = \frac{c_i - c_{i-1}}{\Delta x_{i-1}}, \tag{32}$$

where $\Delta x_{i-1} = x_i - x_{i-1}$. A piece-wise constant variation is assumed for the spatial-derivative term:

$$\frac{\partial}{\partial \tau}\int_{x'_1}^{x'_{i+1}} cx^2\,\mathrm{d}x = \frac{\mathrm{d}c_i}{\mathrm{d}\tau}\,\frac{x'^3_{i+1} - x'^3_i}{3}. \tag{33}$$

The outcome is a classical tri-diagonal system of equations that can be solved for the unknown values c_i. This type of system is quickly solved by the well-known TDMA algorithm.

This type of discretization is akin to finite differencing and is known to have rather poor convergence properties [9,15]. It needs a rather large number of mesh points, particularly at low release. In order to increase the accuracy of the method, a new higher-order scheme has been developed and is addressed in the following section.

3.2.2. Higher-order scheme

This is the highest-order scheme for the derivative terms that is compatible with the tridiagonal system structure. Namely, a linear variation is assumed everywhere for the concentration except at end-volumes where a quadratic variation is assumed. Then, for $i \neq 1,\ 2,\ N_{x-1},\ N_x$, Eq. (31) holds and Eq. (33) is replaced by

$$\begin{aligned}\frac{\partial}{\partial \tau}&\int_{x'_i}^{x'_{i+1}} cx^2\,\mathrm{d}x \\ &= \frac{\mathrm{d}c_{i-1}}{\mathrm{d}\tau}\int_{x_i}^{x'_{i+1}} \frac{x_i - x}{\Delta x_{i-1}}x^2\,\mathrm{d}x + \frac{\mathrm{d}c_i}{\mathrm{d}\tau} \\ &\quad\times\left[\int_{x'_i}^{x_i}\frac{x - x_i}{\Delta x_{i+1}}x^2\,\mathrm{d}x\int_{x_i}^{x'_{i+1}}\frac{x - x_i}{\Delta x_i}x^2\,\mathrm{d}x\right] \\ &\quad+ \frac{\mathrm{d}c_{i+1}}{\mathrm{d}\tau}\int_{x_i}^{x'_{i+1}}\frac{x_{i+1} - x}{\Delta x_i}x^2\,\mathrm{d}x.\end{aligned} \tag{34}$$

For control-volume 1, $\partial c/\partial x = 0$ at $x = 0$, and the quadratic variation assumption yields

$$\begin{aligned}\frac{\partial c}{\partial \tau}&\int_0^{x'_2} cx^2\,\mathrm{d}x \\ &= \frac{\mathrm{d}c_1}{\mathrm{d}\tau}\left[\int_0^{x'_2}\frac{x_2^2}{x_2^2 - x_1^2}x^2\,\mathrm{d}x - \int_0^{x'_2}\frac{x^4\,\mathrm{d}x}{x_2^2 - x_1^2}\right] \\ &\quad+ \frac{\mathrm{d}c_2}{\mathrm{d}\tau}\left[\int_0^{x'_2}\frac{x^4\,\mathrm{d}x}{x_2^2 - x_1^2} - \int_0^{x'_2}\frac{x_1^2}{x_2^2 - x_1^2}x^2\,\mathrm{d}x\right]\end{aligned} \tag{35}$$

and the spatial-derivative term is

$$x'^2_2\left.\frac{\partial c}{\partial x}\right|_{x'_2} = -\frac{2x'_2}{x_2^2 - x_1^2}c_1 + \frac{2x'_2}{x_2^2 - x_1^2}c_2. \tag{36}$$

Similar expressions can be derived for control-volume N_x where a quadratic variation can be assumed and where the end-concentration, c_S, at $x = 1$ is known. However, the quadratic-variation algorithm did not improve significantly the results for the test cases over the linear-variation algorithm. This result indicates that the spatial derivative at the grain boundary ($x = 1$) is not more accurately approximated by the quadratic variation than by the linear variation. In the following, only the results for the linear variation of the spatial derivative will be presented.

3.3. Time discretization

The time-derivative term is discretized with the backward Euler approximation:

$$\frac{\mathrm{d}c_i}{\mathrm{d}\tau} = \frac{c_i^{n+1} - c_i^n}{\Delta\tau}, \tag{37}$$

where superscripts n and $n+1$ represent the beginning and the end of a time-step, respectively. The spatial-derivative terms are fully implicit:

$$\left.\frac{\partial c}{\partial x}\right|_{x'_i} = \frac{c_i^{n+1} - c_{i-1}^{n+1}}{\Delta x_{i-1}}, \tag{38}$$

thus ensuring numerical stability.

With the combination of the previous spatial scheme and this time scheme, for a constant increment Δx, higher-order terms are minimized when the following condition is fulfilled:

$$\Delta\tau = C_x \Delta x^2 \tag{39}$$

where C_x is the condition number found by varying $\Delta\tau$ until error minimization is achieved.

In our case of variable spatial increments, we generalize the previous formula for given test cases by searching for the optimal value, $\Delta\tau_{\mathrm{OPT}}$:

$$\Delta\tau_{\mathrm{OPT}} = C_x \Delta x_{N_x}^2. \tag{40}$$

In fuel rod design computer codes like TRANSURANUS [29], the time-step, $\Delta\tau_{\mathrm{CODE}}$, is common to all physical models. It is managed by finding the smallest time-step that is compatible for numerical stability and/or precision of the models. The following strategy is proposed for such codes: if $\Delta\tau_{\mathrm{CODE}} < \Delta\tau_{\mathrm{OPT}}$, compute the concentrations with $\Delta\tau_{\mathrm{OPT}}$ and interpolate for $\Delta\tau_{\mathrm{CODE}}$,, otherwise impose $\Delta\tau_{\mathrm{CODE}} = \Delta\tau_{\mathrm{OPT}}$. This strategy, that is discussed in the next Section, proved to be efficient.

Once discretized with this double choice of space and time discretization, the diffusion equation symbolically reads

$$\left(\frac{A}{\Delta\tau} + B\right)c^{n+1} = \frac{A}{\Delta\tau}c^n + P, \tag{41}$$

where A and B are tridiagonal matrices.

4. Results

4.1. Introduction

Simple cases are presented initially before the full problem of time-varying conditions as well as time-vary-

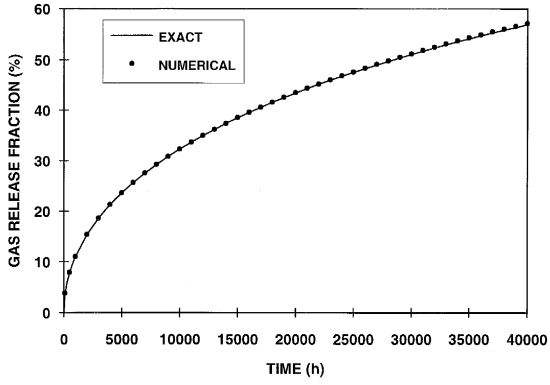

Fig. 2. Gas release fraction versus time for constant gas production, zero concentration at the boundary and $D/a^2 = 7.1 \times 10^{-10}$ s^{-1}.

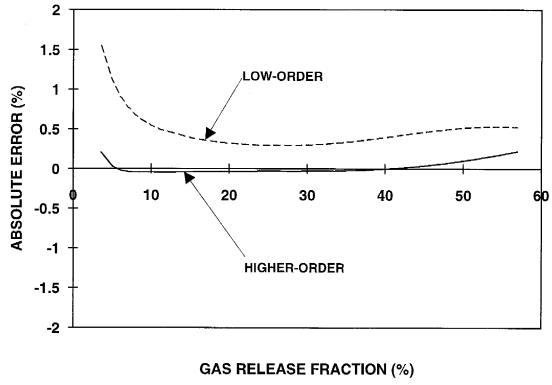

Fig. 3. Absolute error for 10 low-order and 10 high-order finite-volumes and the case of Fig. 2.

ing boundary conditions is presented. For steady-state conditions, analytical solutions exist that can be compared with predictions. The first case represents constant gas production and a perfect sink. This case is relevant to steady-state LWR operation (except for the perfect sink condition). The second case represents zero gas production and a perfect sink. This case is relevant to power transients when the diffusional release dominates the gas production. The third case represents constant gas production with an imperfect sink. This case is similar to the first case but is more realistic.

4.2. Steady-state conditions

4.2.1. Perfect sink with gas production

In this case,

$$\beta = \text{constant}, \qquad c(r, 0) = 0, \qquad c(a, t) = 0. \tag{42}$$

Booth [3] found an analytical expression for the release fraction, F:

$$F(t) = 1 - \frac{6}{Dt/a^2}\left[\sum_{n=1} \frac{1 - \exp(n^2\pi^2 Dt/a^2)}{n^4\pi^4}\right]. \tag{43}$$

Fig. 2 presents a comparison between the analytical solution (Eq. (43)) and predictions made with 10 higher-order finite volumes. Typical LWR steady-state operations were chosen, namely, $T = 900°C$, $P' = 20$ kW/m. From Eqs. (1)–(7), $D = 1.78 \times 10^{-20}$ m^2/s and a grain size with radius $a = 5 \times 10^{-6}$ m was assumed. The irradiation range extends to about 70 000 MWd/tM.

Fig. 3 illustrates the absolute error

$$\Delta F(\%) = F_{\text{NUM}}(\%) - F_{\text{ANAL}}(\%), \tag{44}$$

where F_{NUM} is the result of computations and F_{ANAL} is the analytical expression (Eq. (43)). F_{NUM} was derived with the relation

$$F_{\text{NUM}} = 100\left(1 - \frac{\int_0^1 cx^2\,\mathrm{d}x}{\int_0^\tau \mathrm{d}\tau' \int_0^1 \beta' x^2\,\mathrm{d}x}\right), \tag{45}$$

where the higher-order spatial variation is assumed for c. Fig. 3 also presents a comparison of the predictions obtains with 10 low-order finite-volumes and clearly demonstrates the improvement in accuracy achieved by going from the low-order to the higher-order spatial scheme. Note the error becomes larger at low releases. This is of no importance because, with this simple case, low release occurs at the very early stage of irradiation (< 100 h) in typical LWR steady-state operation.

Fig. 4 illustrates how the absolute error varies with the condition number C_x for 10 higher-order finite-volumes. An optimal choice with $C_x \sim 0.2$ was found. The error is below 0.2% over the entire irradiation range with this value of the condition number.

The minimum number of finite-volumes that are compatible with a required bound for the error will now be determined. Fig. 5 shows the error calculated for different numbers of finite-volumes and with a condition number of 0.2 (this condition number was found to be optimal irrespective of the number of finite-volumes). Except at the very early stage of irradiation, three finite-volumes are

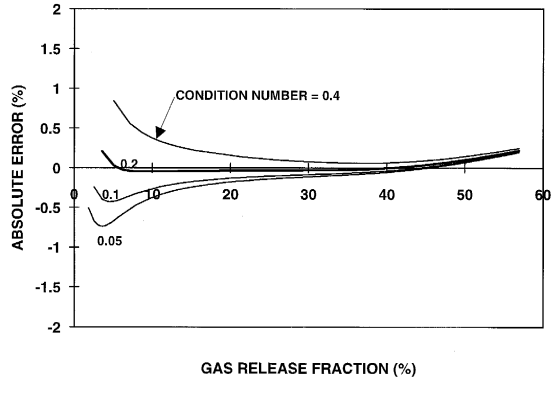

Fig. 4. Variation of the absolute error with time-step for 10 high-order finite-volumes and the case of Fig. 2.

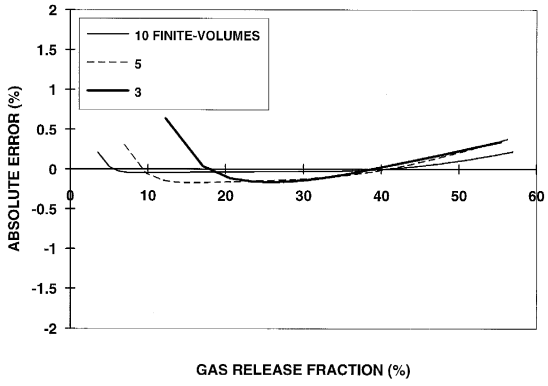

Fig. 5. Variation of the absolute error with the number of finite-volumes for the case of Fig. 2.

sufficient for good accuracy. This number is identical to the number of quadratic finite-elements used in Ref. [9].

4.2.2. Perfect sink without gas production

Except for the perfect sink condition, this case is relevant to LWR Class-I and Class-II type conditions. The diffusion Eq. (26) is solved with the following conditions:

$$\beta = 0, \qquad c(r, 0) = \text{constant} = c_0, \qquad c(a, t) = 0. \tag{46}$$

This problem has the following analytical solution [3]:

$$F(t) = 1 - 6 \sum_{n=1} \frac{\exp(-n^2\pi^2 Dt/a^2)}{n^2\pi^2}. \tag{47}$$

The following conditions, typical of an upper-bound limit of all Class-I conditions wee chosen for this test case: $T = 1500°C$, $P' = 40$ kW/m, $D = 3.2 \times 10^{-17}$ m^2/s, and transient length equal to 10 h. For an upper-bound limit of all Class-II incidents, the power is slightly higher, but the transient length is shorter, resulting in less release. Fig. 6 presents a comparison between the analytical expression (Eq. (47)) and numerical computations made with 10 and 3 high-order finite-volumes. Again, a condition number equal to 0.2 was used. As before, three finite-volumes are sufficient for good accuracy.

With three finite-volumes, the optimum choice for the previous constant gas production case is $\Delta t = 1240$ h, which is greater than typical time-step values of fuel rod design computer codes (of the order of 100 h). Therefore, the strategy $\Delta\tau_{\text{CODE}} < \Delta\tau_{\text{OPT}}$ holds.

For this case, $\Delta t = 0.75$ h and the other alternative strategy $\Delta\tau_{\text{CODE}} = \Delta\tau_{\text{OPT}}$ is likely to hold.

4.2.3. Imperfect sink

The diffusion equation is solved with the following boundary conditions:

$$\beta = \text{constant}, \qquad c(r, 0) = \text{constant} = c_0,$$
$$c(a, t) = c_\delta = (bN_s\delta)/(2D). \tag{48}$$

The solution is [5]

$$F(t) = 1 - \Big[\, \beta/15 + c_\delta + 6\Sigma_{n=1}\big((c_0 - c_\delta)/(n^2\pi^2) - \beta/(n^4\pi^4)\big)\exp(-n^2\pi^2 Dt/a^2) \Big/ \big(c_0 + \textstyle\int_0^t \beta\, dt'\big)\Big]. \tag{49}$$

The same irradiation conditions as the perfect sink test case of Section 4.2.1 were chosen. Additional conditions are for c_0 and c_δ: $c_0 = 2.15 \times 10^{26}$ m^{-3} (gas production after 20 000 h of irradiation) and $c_\delta = 3.15 \times 10^{25}$ m^{-3}. Fig. 7 is similar to Fig. 6 and the conclusions are identical: three finite-volumes give good accuracy.

4.3. Time-varying conditions

4.3.1. Perfect sink

The algorithm will now be tested for time-varying conditions, with a perfect sink boundary condition (this Sub-Section), and then, with an imperfect sink condition

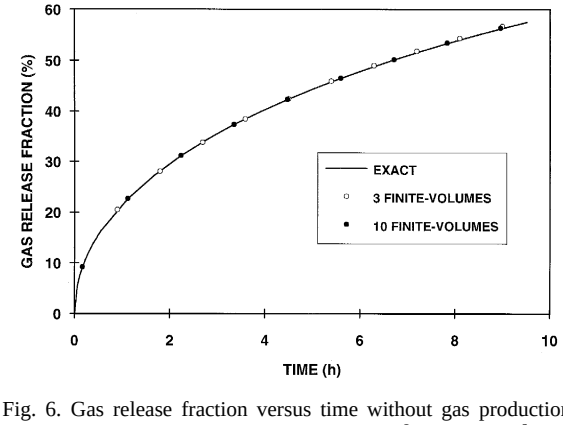

Fig. 6. Gas release fraction versus time without gas production, zero concentration at the boundary and $D/a^2 = 1.3 \times 10^{-6}$ s^{-1}.

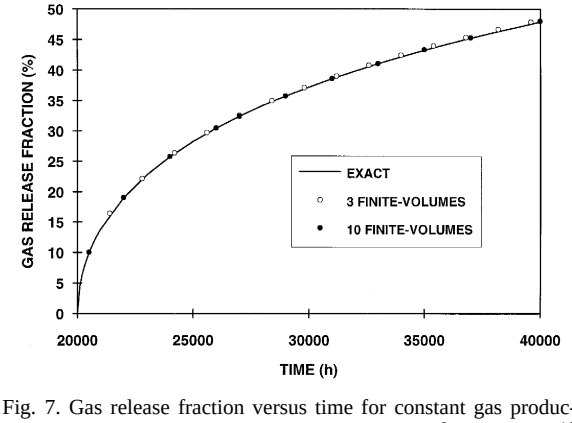

Fig. 7. Gas release fraction versus time for constant gas production, finite concentration at the boundary $D/a^2 = 7.1 \times 10^{-10}$ s^{-1}, $N_S = 2.5 \times 10^{20}$ m^{-2} and $b = 10^{-6}$ s^{-1}.

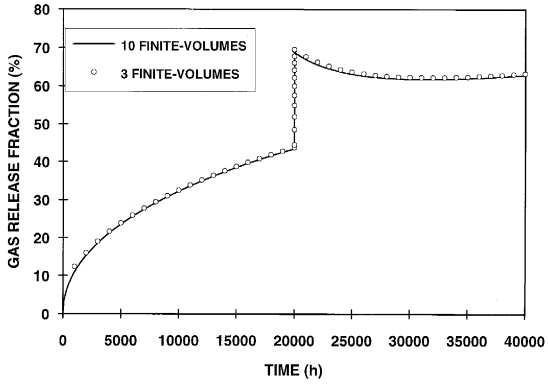

Fig. 8. Gas release fraction versus time for time-varying conditions and zero concentration at the boundary.

(next Sub-Section). As mentioned before, the time-varying operating condition of most interest is a power transient that represents an upper-bound of Class-I conditions. A test case with irradiation conditions made up of 5 time intervals is presented. Time intervals 1 and 5 represent steady-state operations with $T = 950°C$ and $P' = 25$ kW/m. The power transient lasts during time intervals 2 (ramping-up phase), 3 (high power hold phase) and 4 (ramping-down phase). Time intervals 2 and 4 are 1 h. Time interval 3 is 10 h. Conditions for interval 3 are the same as those in Section 4.2.2 except that gas production is now finite.

Fig. 8 shows the evolution of the gas release fraction. Again, 3 higher-order finite-volumes are enough for good accuracy. The time-step management has been studied. The interpolation scheme described in Section 3.3 has been refined. With the above-mentioned conditions during steady-state, the time-step is equal to 1240 h for a condition number of 0.2 and 3 higher-order finite-volumes. This value is more than 10 times larger than the typical value found in fuel rod design computer codes (about 100 h). Direct interpolation, for that reason, gives a slightly inaccurate value. However, when the second derivative of the concentration with respect to time is negative, direct interpolation under-estimates the value of the concentration. On the other hand, Figs. 2–5 show that with a condition number less than 0.2, the values of the concentration are over-estimated. Hence, we have tested the following algorithm:

$$c^{n+1} = 0.5\left(c_1^{n+1} + c_2^{n+1}\right), \tag{50}$$

where c_1^{n+1} is evaluated with time-step $\Delta\tau_{\mathrm{CODE}}$ and c_2^{n+1} is obtained by linear interpolation (or extrapolation) from $\Delta\tau_{\mathrm{OPT}}$ to $\Delta\tau_{\mathrm{CODE}}$:

$$c_2^{n+1} = \left[c^{n+1}\Delta\tau_{\mathrm{CODE}} + c^{n}\left(\Delta\tau_{\mathrm{OPT}} - \Delta\tau_{\mathrm{CODE}}\right)\right]/\Delta\tau_{\mathrm{OPT}}. \tag{51}$$

This time-step algorithm was adopted (using $\Delta\tau_{\mathrm{CODE}} =$ 100 h during intervals 1 and 5) for Fig. 8 and, as shown, yields good results.

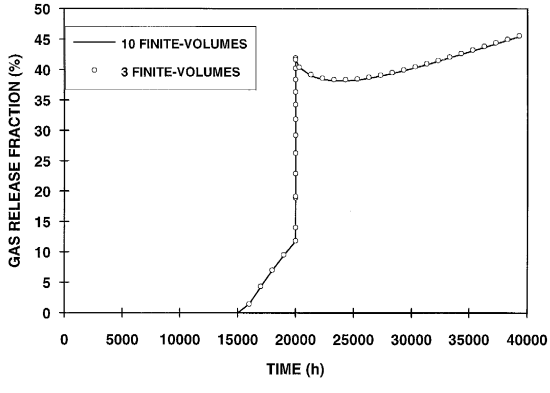

Fig. 9. Gas release fraction versus time for time-varying conditions and finite concentration at the boundary.

4.3.2. Imperfect sink

The conditions for this case are the same as those of Section 4.3.1, except, now, the boundary condition is given by Eq. (8). Below saturation ($N < N_{\mathrm{S}}$), the surface density N is numerically evaluated through the mass balance equation (gas production is then equal to the amount of gas inside the grain and on the grain boundary):

$$\int_0^1 cx^2\,\mathrm{d}x + \frac{1}{2}\frac{N}{a} = \int_0^{\tau}\mathrm{d}\tau'\int_0^1 \beta' x^2\,\mathrm{d}x. \tag{52}$$

An iteration scheme is used and stops at iteration j whenever

$$|N^{i+1} - N^{i}|/N^{i+1} \le 0.01. \tag{53}$$

In practice, two iterations were sufficient for convergence.

The saturation value N_{S} is obtained when the burnup of the incubation curve (Fig. 1) is reached. Fig. 9 illustrates the evolution of the gas release fraction. In the test case, N_{S} has been assumed constant for the purpose of illustration. Obviously, a more complicated law could be used that includes a temperature and pressure dependence, and even more, a kinetic evolution. The refined time-step algorithm defined in the previous Section was used to generate the curves of Fig. 9. This algorithm, together with only 3 higher-order finite-volumes, yields good results.

5. Discussion

5.1. Comparison with other algorithms

For the steady-state case, Refs. [12,13] use the semi-analytical approximation (Eq. (49)) where, now,

$$c_0 = \beta t_i - 3N_{\mathrm{S}}/2a \tag{54}$$

and t is replaced by $t - t_i$ in the exponential term. Fig. 10 presents a comparison between this approximation and the numerical scheme for the steady-state irradiation conditions used in Section 4.3.1. Results shown in Fig. 10 and in Ref. [12] are virtually identical (see for instance fig. 10 in Ref. [12]). This approximation over-estimates the gas release fraction. This over-estimation is more pronounced at low release values and is less than 3% at the highest release value. The approximation, in effect, smears out the initial concentration profile at incubation. Hence, the initial concentration gradient at the boundary is too steep and induces an initial release too quickly.

The physical model [12] is similar to the model presented in this paper. The major difference is that the incubation is prescribed in the present model and the density at saturation, N_S, is numerically deduced from the mass balance Eq. (52). In Ref. [12], N_S, was prescribed and then, the incubation curve was deduced by solving the approximate equation, Eq. (13). Other differences come from the numerical treatment. In Ref. [12], finite differences were used. Also, re-solution was treated as a boundary layer whose thickness was 2δ. That is, the gas production in the boundary layer, β_{BL}, was $\beta_{BL} = \beta + bN/4\delta$, and the boundary condition remained $c(a,\ t) = 0$. This approach required 100 mesh points, as mesh accumulation close to the boundary was needed, due to the small value of $\delta \sim 10^{-8}$ m. From the previous discussion, a small mesh size also limits the time-step. The finite difference scheme was improved by using finite elements [14] (10 finite elements only were needed for good convergence). However, in Ref. [14] like in Ref. [12], the boundary layer approach is somewhat penalizing. On the other hand, the similarity between the results presented here and those of Ref. [12] indicate that both approaches are nearly equivalent.

Another approximation in the case of a transient has been tested. It consists of neglecting the gas production

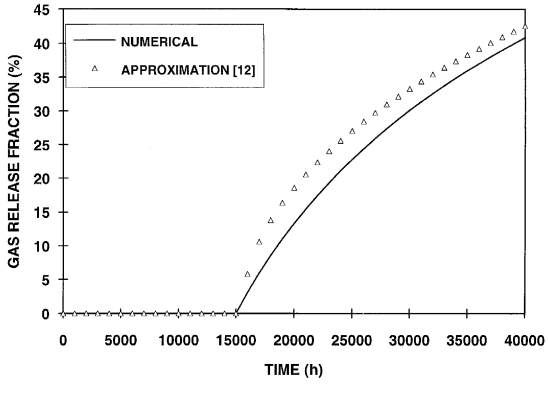

Fig. 10. Gas release fraction versus time for constant gas production. Comparison between finite-volume calculations and the semi-analytical approximation used in Ref. [12].

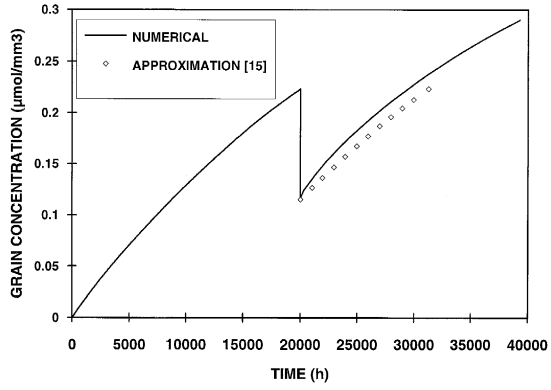

Fig. 11. Grain volume average concentration versus time for time-varying conditions. Comparison between finite-volume calculations and the semi-analytical approximation used in Ref. [15].

during the transient. The approximation then becomes a generalization of Eq. (47)

$$\langle c\rangle = \langle c\rangle_{INI} 6 \sum_{n=1} \frac{1}{n^2\pi^2} \exp\left[-n^2\pi^2 \int_{t_{INI}}^{t} D\,\mathrm{d}t/a^2\right], \tag{55}$$

where $\langle c\rangle$ is the grain volume average of the concentration, t_{INI} is the time when the transient begins and $\langle c\rangle_{INI}$ is the concentration at t_{INI}. For example, with this approximation, the gas release fraction is over-estimated by 7% at the end of the transient shown in Fig. 9. The approximation has the same smearing-out effect on the initial concentration profile as mentioned before.

A third approximation was proposed in Ref. [15]: the evolution of $\langle c\rangle$ from a given time t_0 follows the evolution of $\langle c\rangle$ at an equivalent time. This equivalent time is given by the time needed to reach the value of $\langle c\rangle$ at t_0 assuming the temperature level is constant and equal to the value at t_0. Fig. 11 compares the evolution of $\langle c\rangle$ between this approximation and numerical scheme for the case of Section 4.3.2, starting at the beginning of interval 5. Again, this approximation over-estimates the gas release as it smears out the concentration profile.

5.2. Computer time

This fission gas release model has been implemented in the version of the fuel rod computer code TRANSURANUS [29] used at Framatome. The computer time used by the model has been measured. It is about 10% of the computer time used by the code. This number applies to the reference numerical scheme that consists of 3 higher-order finite-volumes, 2 iterations for convergence of the boundary concentration, and 2 time-steps per code time-step, following Eq. (51). The relative low time spent in calculating fission gas makes the numerical scheme presented here attractive.

6. Conclusion

A model for thermally-activated fission gas release from UO_2 fuel has been developed. The model includes relevant physical phenomena such as the diffusion of fission gas from the UO_2 grain interior to the grain boundary, re-solution within the grain and grain boundary, and gas saturation at the grain boundary.

The problems were numerically solved by applying a finite-volume method. The method was optimized for LWR operations (within Class-I and Class-II limits). A new space and time discretization scheme was found. There is an excellent agreement between the numerical computations and the known analytical results that pertain to time-independent conditions. The method is efficient for application in fuel rod design computer codes because the computer time spent in the fission release calculations is typically 10% of the total computer time.

References

[1] D.R. Olander, Fundamental Aspects of Nuclear Reactor Fuel Elements, ERDA, USA (1974).
[2] C. Vitanza, E. Kolstad and U. Graziani, Fission Gas Release from UO_2 Pellet Fuel at High Burn-up, ANS Topical Meeting on LWR Fuel Performance, Portland, WA, USA (1979) p. 361.
[3] A.H. Booth, A Method of Calculating Fission Gas Diffusion from UO_2 Fuel and its Application to the X-2-f Loop Test, Rapport Atomic Energy of Canada Limited CRDC-721 (1957).
[4] M.V. Speight, Nucl. Sci. Eng. 31 (1969) 180.
[5] J.A. Turnbull, J. Nucl. Mater. 50 (1974) 62.
[6] R. Hargreaves and D.A. Collins, J. Brit. Nucl. Energy Soc. 15 (1976) 311.
[7] W.N. Rausch and F.E. Panisco, ANS54: A Computer Subroutine for Predicting Fission Gas Release, NUREG/CR-1213 (1979).
[8] C.S. Rim, Background and Derivation of ANS-5.4 Standard Fission Product Release Model, NUREG/CR-2507 (1982) p. 19.
[9] J.R. Mattews and M.H. Wood, Nucl. Eng. Des. 56 (1980) 439.
[10] H. Mertins and M. Pluff, J. Nucl. Mater. 92 (1980) 217.
[11] L. Vath, J. Nucl. Mater. 99 (1981) 324.
[12] D.M. Dowling, R.J. White and M.O. Tucker, J. Nucl. Mater. 110 (1982) 37.
[13] R.J. White and M.O. Tucker, J. Nucl. Mater. 118 (1983) 1.
[14] K. Ito, R. Iwasaki and Y. Iwano, J. Nucl. Sci. Technol. 22 (1985) 129.
[15] P.T. Elton and K. Lassmann, Nucl. Eng. Des. 101 (1985) 259.
[16] K. Forsberg and A.R. Massih, J. Nucl. Mater. 127 (1985) 141.
[17] K. Forsberg and A.R. Massih, J. Nucl. Mater. 135 (1985) 140.
[18] K. Forsberg, F. Lindström and A.R. Massih, Modelling of Some High Burnup Phenomena in Nuclear Fuel, IAEA Technical Committee Meeting on Water Reactor Fuel Element Modelling at High Burnup and Experimental Support, Windermere, UK (1994).
[19] J.B. Ainscough, B.W. Oldfield and J.O. Ware, J. Nucl. Mater. 49 (1973) 117.
[20] M. Paraschiv and A. Paraschiv, J. Nucl. Mater. 185 (1991) 182.
[21] U.M. El-Saied and D.R. Olander, J. Nucl. Mater. 207 (1993) 313.
[22] J.A. Turnbull, C.A. Friskney, J.R. Findlay, F.A. Johnson and A.J. Water, J. Nucl. Mater. 107 (1982) 168.
[23] J.A. Turnbull, R.J. White and C. Wise, The Diffusion Coefficient for Gission Gas Atoms in Uranium Dioxide, IAEA Tech. Com. Meeting on Water Reactor Fuel Element Computer Modelling in Steady State, Transient and Accident Conditions, Preston (1988).
[24] Hj. Matzke, Radiat. Eff. 53 (1980) 219.
[25] C. Bernaudat, Nucl. Eng. Des. 156 (1995) 373.
[26] C.T. Walker, P. Knappik and M. Mogensen, J. Nucl. Mater. 160 (1988) 10.
[27] H. Zimmermann, J. Nucl. Mater. 75 (1978) 154.
[28] I.R. Brearly and D.A. Mac Innes, J. Nucl. Mater. 95 (1980) 239.
[29] K. Lassmann and H. Blank, Nucl. Eng. Des. 106 (1988) 291.